1 Rupture propagation along stepovers of strike-slip faults: Effects of initial

2 stress and fault geometry

- 3 Hui Wang¹, Mian Liu², Benchun Duan³, Jianling Cao¹
- 4 1- Institute of Earthquake Forecasting, China Earthquake Administration, Beijing 100036,
- 5 China
- 6 2- Dept. of Geological Sciences, University of Missouri, Columbia, MO 65211, USA
- 7 3- Center for Tectonophysics, Department of Geology and Geophysics, Texas A&M
- 8 University, College Station, TX 77843, USA

Abstract

Large earthquakes on strike-slip faults often rupture multiple fault segments by jumping over stepovers. Previous studies, based on field observations or numerical modeling with a homogeneous initial stress field, have suggested that stepovers more than ~ 5-km wide would stop the propagation of rupture, but many exceptions have been observed in recent years. Here we integrate a dynamic rupture model with a long-term fault stress model to explore the effects of background stress perturbation on rupture propagation across stepovers along strike-slip faults. Our long-term fault models simulate steady-state stress perturbation around stepovers. Considering such stress perturbation in dynamic rupture models leads to prediction of larger distance a dynamic rupture can jump over stepovers: over 15-km for a releasing stepover or 7-km for a restraining stepover, comparing with the 5-km limit in models with the same fault geometry and frictional property but assuming a homogeneous initial stress. The effect of steady-state stress perturbations is stronger in an overlapping stepover than in an underlapping stepover. The maximum jumping distance can reach 20 km in an overlapping releasing stepover with low static frictional coefficients. These results are useful for estimating the maximum length of potential fault ruptures and assessing seismic hazard.

Introduction

27

28

29

30

31

32

33

34

35

36

37

38

39

40

41

42

43

44

45

46

47

48

49

50

51

Large earthquakes, especially those on continental strike-slip faults, usually rupture multiple fault segments by propagating fault rupture across stepovers. Recent examples include the 1992 Mw7.3 Landers, California, earthquake (Wald and Heaton, 1994), the 2001 Mw7.8 Kokoxili, China, earthquake (Xu et al, 2002), the 2016 Mw6.5 Norcia, Italy, earthquake (Scognamiglio et al., 2018), and the 2016 Mw7.8 Kaikoura, New Zealand, earthquake (Kaiser et al, 2017). When stepovers are too wide, fault rupture might stop there. Thus stepovers are common sites where large strike-slip fault ruptures terminate (Wesnousky, 2006). Knowing whether or not a stepover can arrest fault rupture is critical for determining the maximum magnitude of potential earthquakes in a fault system, a key parameter in seismic hazard assessment (Kijko and Selleboll, 1989; Field et al, 2014). Previous studies, based on limited amount of field observations and numerical models of dynamic rupturing (e.g., Harris and Day, 1993; Lozos et al., 2011; Wesnousky, 2006), suggest that propagation of fault rupture would stop at stepovers where fault segments are separated more than ~ 5 km. Numerous exceptions have been observed in recent years. In particular, the 2016 Mw7.8 Kaikoura, New Zealand, earthquake ruptured 13 faults, with step gaps as large as 15-20 km (Hamling et al., 2017; Kaiser et al, 2017; Ulrich et al., 2019). These new observations call for reevaluation of earthquake hazard assessment in many regions (Hamling et al., 2017). Whereas past earthquakes provide empirical estimations of the maximum step size through which an earthquake might rupture (Biasi and Wesnousky, 2016), the number of good measured surface ruptures are limited, and cases with larger jumping step widths may be missed. Estimates based on dynamic rupture models, on the other hand, depends on many parameters, most importantly the initial stress, fault geometry, and frictional property (Harris et al., 2009). The initial stress, however, is hard to constrain, so a homogeneous initial stress is usually assumed in previous dynamic rupture models, although it is well known from field studies that stepover and other fault irregularities can significantly change the local stress field (Sylvester, 1988; Cunningham and Mann, 2007; Mann, 2007). Models of long-term fault tectonics also show significant stress variations near stepovers (McClay and Bonora, 2001; Ye et al., 2015; Wang et al., 2017; Wijk et al., 2017). Whereas variations of fault geometry across stepovers have been explored in previous studies for their impact on rupture propagation (Sibson, 1985; Kase and Kuge, 2001; Wesnousky, 2006; Lozos et al., 2011), systematic investigation is needed in light of the recent observations of rupture jumping over wide stepovers. Furthermore, frictional coefficients could affect rupture propagating on strike-slip fault (Aochi et al., 2002; Lozos et al., 2014; Liu and Duan, 2015), hence their impact need to be studied together with those of the initial stress and fault geometry.

In this study, we first investigate stress perturbation near stepovers in a 3-D numerical model of long-term fault stress. The results are then incorporated in a 2-D model of dynamic ruptures to systematically explore the propagation of fault ruptures over stepovers with various initial stress and fault geometry. We attempt to address two key questions: 1) What is the maximum stepover width for fault rupture to jump over in a more realistic stress field? 2) How would the initial stress, stepover geometry, and frictional property affect the maximum jumping distance?

Models and Methods

In this paper, we firstly use a three-dimensional (3D) viscoelasto-plastic finite element code (Li and Liu, 2006; Li et al., 2009) to calculate stress perturbation around stepovers. We then use the results to constrain the initial stress in a 2-D dynamic rupture model (Duan and Oglesby, 2006; Duan and Day, 2008) to investigate rupture propagation over stepovers with various fault geometry and frictional fault properties.

Stress perturbation around stepovers

76

77

78

79

80

81

82

83

84

85

86

87

88

89

90

91

92

93

94

95

96

97

98

99

Figure 1 shows the model setting for simulating steady-state stress perturbation near a stepover that separates the two segments of a strike-slip fault. To minimize edge effects, a large model domain (200 km long and 100 km wide) is used. The model lithosphere includes two rheological layers: a 20-km thick brittle (elastoplastic) upper crust and a 40-km thick viscoplastic lower crust and upper mantle (Figure 1a). The faults cut through the entire upper crust, and are modeled as 400-m thick vertical layers of fault elements with lower strength than that of the surrounding crust. We used the Drucker-Prager model (Drucker and Prager, 1952) for plastic yield, which is controlled by the values of cohesion and internal friction. Plastic yielding of fault elements with near zero internal friction simulates long-term fault creep. Material parameters in this model take conventional values (Table 1) that are similar to previous studies (Wang et al., 2017). The model domain is fixed on its back side and loaded by imposing a 5 mm/yr velocity on its front side. This is half of the typical values of slip rate on major intracontinental strike-slip faults (Molnar and Dayem, 2010) (Figure 1a). Depending on the direction of the imposed velocity, the stepover can be compressive (restraining) or extensional (releasing). The left and right sides of the model domain are free to move in the direction along the fault strike but fixed in other directions; this prevents block rotation. The top surface is free; the bottom is free to move in the horizontal direction and fixed in the vertical direction. Stress evolution in the model is simulated using a finite element method as detailed in previous studies (Li and Liu, 2006; Liu et al., 2010; Wang et al., 2017; Ye and Liu, 2017). We start the numerical simulations with zero stress. Stress increases gradually by the imposed motion on the front side of the model domain until the plastic yields of the fault and the upper crust are reached. Further loading is accommodated by plastic creeping on the fault, and the system enters a steady state.

Figure 2 shows how the stress field is perturbed around a stepover. Because the fault segments are parallel to the x-direction, σ_{yy} and σ_{xy} are the normal and shear stresses on the fault segments, respectively. The results show stress localization around the stepover: high extensional normal stress (σ_{yy}) around the releasing stepover (Figure 2a), and compressive normal stress around the restraining stepover (Figure 2b). Elevated shear stress (σ_{xy}) is localized near the two fault tips, stronger for the restraining stepover (Figure 2c-d).

Figure 3 shows the vertical distribution of the perturbing normal and shear stresses on the plane of the left fault segment. Near the stepover, extensional (positive) normal stress is elevated for the releasing stepover (Figure 3a), and compressive (negative) normal stress for the restraining stepover (Figure 3b). The restraining stepover also causes higher shear stress than the releasing stepover (Figure 3c-d). The absolute values of the stress perturbation depend on the model parameters, but the spatial patterns of stress perturbation shown in Figures 2-3 are consistent for all reasonable ranges of model parameter values.

Initial stress for dynamic rupture models

The predicted steady-state stress perturbation around stepovers can be used to improve the initial stresses assigned in models of dynamic ruptures. We need to point out that the spatial patterns of stress perturbation around stepovers are more meaningful than the specific stress values, which depend on model parameters including the width of the stepover. To incorporate the steady state stress perturbation into dynamic rupture models and to compare their impact on stepovers with various stepover widths, we normalize the steady-state stress perturbation by the dynamic stress drop ($\Delta \tau$) in ruptures. First, we modeled the stress fields around stepovers that are from 1 km to 20 km wide while keeping all other model parameters and boundary

constrains the same. Then, we normalize the normal stress σ_N and shear τ on the fault planes from steady-state models using the assumed stress drop ($\Delta \tau$), based on initial stress and frictional coefficients, in the dynamic rupture model. So the stress perturbation is less than the stress drop ($\Delta \tau$), while the spatial pattern of stress variations is the same as in the steady-state fault stress model. Last, we add the normalized steady-state shear and normal stresses to the shear and normal stress value from the homogeneous case, respectively. The process makes all cases with different stepover width comparable.

Figure 4 shows an example of the initial stresses, respectively for a releasing and a restraining stepover, that are used for the dynamic rupture models. The stress variations near the stepover are based on the results of steady-state fault stress models discussed above. In both cases the stepover is 1 km wide. The maximum variation of the initial stress is scaled to the stress drop ($\Delta\sigma_{max} = \Delta\tau = 10$ MPa) in the reference dynamic rupture model (see below). As shown in Figure 3, stepovers cause more changes in the normal stress than in the shear stress. This variation of initial normal stress affects the dynamic rupture models (see below) by changing the yield stress, which is the product of initial normal stress (σ_0) and the static frictional coefficient (μ_s) on a fault plane. In an overlapping releasing stepover, the yield stress is decreased around the overlapping portion, and increased outside of the overlapping portion (Figure 4a). The opposite is true in an overlapping restraining stepover (Figure 4b). Such a heterogenous initial stress field would affect the initiation and propagation of rupture across the stepovers, as detailed below.

A Two-dimensional dynamic rupture model

We use the 2D EQdyna code to simulate rupture propagation across stepovers along a strike-slip fault. We use a 2D rupture model to better illustrate the impact of background stress variations around stepovers, and for easy comparison with the classical 2D models of rupture

around stepovers. The EQdyna code is an explicit finite element computer program (Duan and Oglesby, 2006; Duan and Day, 2008) and is verified in a community-wide effort (Harris et al., 2009, 2011, 2018). In the code a fault is treated as a surface, across which the displacement vector is permitted to have a discontinuity (Day et al., 2005). The traction-at-slip-node scheme (TSN) is used to numerically implement faulting conditions (e.g., Day et al., 2005; Duan 2010). The frictional strength is the product of the frictional coefficient and the normal stress on the fault. And the frictional coefficient evolves during fault slip by following a local coulomb failure criterion and a linear slip-weakening friction law (Andrews, 1976a,b; Andrews, 1985). In our 2D dynamic rupture models, two strike-slip fault segments with a length of 28 km are embedded in a homogenous elastic medium. The nucleation point is located at 14 km away from the right tip of the left fault segment (Figure 1b). We use two parameters to define the geometry of stepovers: the width of the step between two fault segments (W) and the offset angle (α) (Figure 1c). The offset angle indicates overlapping ($\alpha < 90^{\circ}$) or underlapping ($\alpha \ge$ 90°). For comparison, the reference case in our study assumes a homogenous initial stress, fault slip sense, and length similar to those used by (Harris and Day, 1993). In most cases, the static frictional coefficient is set to be 0.75 (Byerlee, 1978), and the dynamic frictional coefficient to be 0.30. Furthermore, a dimensionless parameter that characterizes the relative fault strength, S value, is considered. The S value is defined as $S = (\tau_v - \tau_0)/(\tau_0 - \tau_f)$, where $\tau_v = \sigma_0 \mu_s$ and $\tau_f = \sigma_0 \mu_d$ are static shear strength and dynamic shear strength, respectively; σ_0 and τ_0 are initial normal stress and shear stress, respectively, and μ_s and μ_d are static and dynamic frictional coefficients, respectively. For in-plane shear ruptures, the rupture is typically subshear when the S value is greater than 1.63, but can reach supershear when the S value is less than 1.63 (Andrews, 1976a; Das and Aki, 1977). We use an element size of 50 m in the dynamic rupture models. The

150

151

152

153

154

155

156

157

158

159

160

161

162

163

164

165

166

167

168

169

170

171

172

simulation time step is set as 0.05 s, and total simulation time for each case is 20.0 s. Major parameters in the dynamic rupture model are provided in Table 2.

To explore how far a rupture can jump over a stepover and how fault geometry and frictional property affect the jumping behaviors, we built several groups of models. We first simulate a group of reference models of overlapping stepovers with a homogenous initial stress field. Then, we explore the effects of variable initial stress fields based on the results from our long-term fault stress models, with different fault geometries. Finally, we examine the effect of fault frictional coefficient. The major variables explored in our study are presented in Table 3.

Model results

The Reference Models

We started with a group of reference models (case 1 in Table 1) that are similar to previous studies (Harris and Day, 1993; Liu and Duan, 2014). These cases provide basic patterns of rupture propagation across stepovers, and serve as a reference for investigating the effects of initial stresses, fault geometry, and frictional property.

Figure 5 shows snapshots of rupture propagating on a reference releasing stepover. In this model, rupture initiates on the left fault segment and later jumps to the right fault segment. At 0.100 s, initial rupture slips a critical weakening distance (d₀) at the set nucleation point on the left fault segment (Figure 5a). Shear stress increases on the nodes ahead of slip. Once shear stress on a fault node reaches its yield stress, the fault node fails and the rupture propagates along the fault. At the same time, shear stress on the ruptured fault nodes drops to the dynamic shear strength $\tau_f = \sigma_0 \mu_d$ (Figure 5b). When the rupture propagates to the overlapping portion of the left fault segment (-2.5 km – 2.5 km on the x-axis), dynamic stress changes produced by

the rupture on the left fault affect both shear and normal stresses on the right fault segment (Figure 5c-d). When shear stress on the right fault segment reaches the yield stress, rupture on the right fault is triggered (Figure 5e). As the rupture propagates on the right fault segment, shear stress on the ruptured fault nodes also drops to the level of dynamic shear strength. Meanwhile, the dynamic stress changes produced by rupture on the right fault segment also affect stress on the left fault segment (Figure 5f-h). Once the right fault segment is ruptured completely, shear stress on the whole fault system is near the level of dynamic shear strength, including the overlapping fault portion where the normal stress, hence the yield stress, changes due to slip on both fault segments (Figure 5i). This reference model shows clearly the two-way dynamic interactions of the two fault segments across the stepover. The basic process of rupture propagation is similar on a reference restraining stepover, but the different shear stresses result in different initial location and time of triggered rupture on the right fault segment, as is shown below.

Figure 6 shows the spatiotemporal evolution of accumulated slip on the two segments of the stepover faults for the reference cases. Once rupture on the right fault segment is triggered, slip mainly occurred on that fault segment. The difference between a releasing stepover and a restraining stepover mainly occurs on the right fault segment, where accumulative slip at a given time is larger in a restraining stepover, indicating a faster rupture velocity than that in a releasing stepover.

We have conducted a suite of models to explore the effects of the stepover width on rupture propagation; the results are summarized in Figure 7. The main result is that rupture can jump over a wider releasing stepover (up to 5 km) than a restraining stepover (up to 3 km). There are also some other differences between releasing and restraining stepovers. First, rupture needs more time to be triggered on the right fault segment in a releasing stepover for the same stepover width. Second, rupture on the right fault segments initiates within the overlapping

portion in a releasing stepover. The initiation point migrates toward the tip of the right fault segment when the stepover width increases. In contrast, in a restraining stepover, rupture on the right fault segment initiates outside of the overlapping portion, and moves away from the fault tip when the stepover width increases. These results are consistent with previous studies (e.g., Harris *et al.*, 1991; Harris and Day 1993; Liu and Duan 2014).

228

229

230

231

232

233

234

235

236

237

238

239

240

241

242

243

244

245

246

223

224

225

226

227

Effects of heterogeneous initial stresses

In the reference models we assumed homogeneous initial stress. However, as shown in our long-term fault stress model, a stepover would cause stress perturbation around it (Figures. 2-3). Here we investigate how such perturbed background or initial stress would affect rupture propagation. We show two groups of models with different initial stress variations based on results from the long-term fault models (case 2 in Table 3). We scaled the stress perturbation by the stress drop: the maximum stress perturbation is half of the stress drop ($\Delta \sigma_{max} = 0.5 \Delta \tau =$ 5 MPa) in one group, and is the same as the stress drop ($\Delta \sigma_{\text{max}} = \Delta \tau = 10$ MPa) in the other group. The results are shown in Figure 8. The influence of the heterogenous initial stress field on rupture propagation across the stepover is clear from comparison with Figure 7. Although the propagation of initial rupture on the right fault segment is similar, the rupture can jump wider stepovers when background stress perturbation around the stepover is considered in the models. For a releasing stepover, the maximum jumping distance can reach 13 km with the maximum stress perturbation capped at 5 MPa, and 15 km with the maximum stress perturbation to be 10 MPa, compared with 5 km in the case of homogeneous initial stress (Figure 7). For a restraining stepover, the maximum jumping distance increases to 4 km when the maximum stress perturbation is 5 MPa, and 7 km when the maximum stress perturbation is 10 MPa.

The larger jumping distances across the stepover with variable initial stresses may be understood by examining the S value, which measures how close the initial stress is to failure stress. Overall, inclusion of long-term background stress perturbation around stepovers results in smaller S values near the stepover. It is 0.5 everywhere on the faults in the reference models with homogeneous initial stress, but varies when long-term stress perturbation is considered. At a releasing stepover, the background extensional normal stress is higher, so the yield stress on the overlapping portion of the faults is lower (Figure 4a). This leads to lower S value and promotes rupture on the right fault segment, which initiates near the end of the right fault segment where the S value is relatively low (Figure 8). A restraining stepover causes increase of background compressive normal stress around it, hence increases the S value on the overlapping portion of the faults. However, it also causes extensional normal stress outside the stepover and decreases the S value there (Figure 4b), resulting in a wider jumping distance.

Effects of underlapping fault segments

The degree of over- and underlapping of the fault segments is an important factor to affect stress and strain fields around stepovers (Dieterich and Richards-Dinger, 2010; Micklethwaite et al., 2015; Wang et al., 2017). In our models, underlapping and overlapping are indicated by the offset angle α (Figure 1c). The fault segments underlap when $\alpha \ge 90^{\circ}$. In this section, we discuss the impacts of fault geometry.

Figure 9 is a summary of modeled rupture behavior on underlapping stepovers (case 3) in a homogenous stress field same as that in the reference case (Case 1). The maximum jumping distance is smaller comparing with overlapping stepovers (Figure 7), and decreases with the increase of the offset angle α . The jumping distance also has a narrower range for an underlapping restraining stepover than an underlapping releasing stepover. In addition, rupture

on the right fault segment all initiates near fault tips. These results reflect the weakening of the interaction between the stress fields of the two fault segments as their tips moving further apart. Rupture propagation across an underlapping stepover can be affected by the long-term background stress. Because $\sim 165^{\circ}$ and $\sim 150^{\circ}$ are thought as critical offset angles for rupture

background stress. Because ~165° and ~150° are thought as critical offset angles for rupture propagation and fault evolution (Lozos et al., 2011; Cooke et al., 2013; Hatem, et al., 2015; Biasi and Wesnousky, 2017), we discuss these two cases below (case 4). Comparing with models with a homogenous initial stress (case 3), models with the long-term background stress perturbation allow rupture to jump across a slightly wider underlapping stepover (2 km for ~165° and ~150° offset angles for both releasing or restraining underlapping stepover). These results are consistent with those for overlapping case (case 2).

Effects of frictional coefficients

The static and dynamic frictional coefficients are important parameters in dynamic rupture models. In this section, we explore their effects in models with a homogeneous initial stress field.

Static frictional coefficient

In case 5 (Table 3), we reduced the static frictional coefficient (μ_s) to 0.65 from 0.75 in the reference case. The lower static frictional coefficient produces a larger jumping distance across stepovers: up to 20 km for overlapping releasing stepovers and 9 km for overlapping restraining stepovers (Figure 10a). The maximum jumping distance is also significantly larger for underlapping stepovers (Figure 10b). These effects are due to the lower yield strength (τ_y), which is the product of initial normal stress (τ_0) and the lower μ_s . Reducing μ_s in this case reduces the yield strength to 21.6 MPa from 25.0 MPa in the reference model (case 1, in table 1), hence the fracture criterion is easier to satisfy, and the rupture is easier to propagate. The

results are also consistent with those from previous works (Lozos et al., 2011; Liu and Duan, 2015).

Dynamic frictional coefficient and stress drops

The dynamic stress drop is defined as the difference between the absolute values of initial shear stress and dynamic shear strength, $\Delta \tau = \tau_0 - \tau_f$, where τ_f is dynamic shear strength: $\tau_f = \sigma_0 \mu_d$ (Table 1) (Day, 1982). Because dynamic frictional coefficient affects stress drop when a fault ruptures, it affects rupture propagation (Aochi et al., 2002).

Figure 11 presents results of varying stress drop on rupture propagation across stepovers (case 6). Fault rupture can jump over a wider overlapping stepover when the stress drop is higher (i.e., lower dynamic frictional coefficient). These results are expected, because larger stress drop means larger energy release at the fracture front that overcomes cohesion (Day, 1982). The effects on underlapping stepovers are weaker and depend on the offset angle.

Discussion

To illuminate the basic mechanism of rupture propagation across stepovers, we kept our models simple and generic. The results are generally consistent with previous studies, but provide more insights on the effects of initial stress, fault geometry, and frictional coefficients. In particular, we found that fault rupture can jump stepovers more than 5 km wide under favorable conditions.

Toward an integrated mechanic fault model

Rupture propagation across stepovers on strike-slip faults has been extensively studied through field investigation and numerical modeling. Statistics on limited surficial fault traces suggested that stepovers more than ~5 km wide would stop the propagation of fault rupture

(Wesnousky, 2006), a conclusion supported by numerical models of dynamic rupture. The first 2D numerical simulation of dynamic rupture propagation across stepover was performed by (Harris et al., 1991), and they have later developed a 3D model (Harris and Day, 1999). With the models of parallel vertical strike-slip faults, they found that simulated ruptures could jump as much as 5 km across releasing stepovers, but only half of that for restraining stepovers. The jumping distance also depended on how close the faults were to failure relative to the stress drop. Because the state of pre-stress is unknown, most previous dynamic models assumed a homogenous background stress field.

Effects of heterogenous initial stresses on the ability for rupture to jump over parallel fault were examined in some previous dynamic models. But the stress perturbation examined was mainly that produced by dynamic rupture. For example, one kind of heterogenous initial stress fields was constructed by considering the change of stress orientation along fault (Lozos, 2016; Lozos et al, 2015). Moreover, heterogenous initial stresses for the subsequent earthquake were produced by the sum of resulting stresses from a previous earthquake and stress changes by interseismic tectonic loading in dynamic rupture models (Harris and Day, 1999). Stress perturbation produced by previous earthquakes on the fault system also has significant effects on rupture initiation, propagation, and termination on a strike-slip fault (Duan, 2019; Duan et al., 2019). Rupture propagation can jump across a wider stepover, more than 10 km, if the fault system has historically experienced many earthquakes (Duan and Oglesby, 2005, 2006; Caniven et al., 2017; Shao et al., 2018).

Integration of dynamic rupture modeling with long-term steady-state stress perturbation should improve physical understanding and prediction of earthquake rupture propagation (Olsen et al., 1997). Background stress change around stepovers has been suggested by geological studies and mechanical fault models. Fault irregularities on strike-slip faults are common locations where crustal deformation is concentrated, forming push-up ranges over

restraining stepovers and pull-apart basins over releasing stepovers. Numeral models also provided insights of basic mechanics of stress evolution around stepovers (Wang et al., 2017).

Integrating models of long-term fault evolution with short-term dynamic rupturing is challenging, however, mainly due to the drastically different timescales for these processes.

Our work takes a step toward integrating long-term fault mechanic models with short-term dynamic rupture models. Results from this study show the importance of long-term steady stress variation on rupture propagation across stepovers.

Model limitations

A major objective of this study is to investigate the impact of tectonic background stress variations around stepovers on the behavior of fault ruptures. For this purpose, we choose to use a 2D rupture models to reduce the influence of other parameters, many of which are not well constrained, such as the depth variation of fault planes and spatial variations of frictional properties. Using 2D rupture models also allows us to compare our results with the classical 2D models of rupture over stepovers.

On the other hand, three-dimensional fault geometry has additional effects on the critical jump distance. Major earthquakes on strike-slip faults with large seismogenic depth can jump wider stepovers (Bai and Ampuero, 2017), and the free surface effect also may produce larger critical jump distance (Hu et al., 2016). Rupture is easier to jump between faults dipping toward one another at steeper angles between paralleled thrust faults (Peshette et al., 2019).

Besides the 3D fault variations, other important factors not considered in our 2D dynamic rupture models include the varying d₀, different friction laws, time-dependent pore fluid pressure, connecting faults and intermediate faults, all could further complicate fault rupture propagation (Harris and Day, 1993; Kase and Kuge, 2001; Duan and Oglesby, 2006, 2007;

Oglesby, 2008; Lozos et al., 2011, 2012, 2014; Ryan and Oglesby, 2014; Luo and Duan, 2018). For examples, decreased effective normal stresses due to increased pore pressure in a restraining stepover may increase or decrease the jumping ability of rupture (Harris and Day, 1993; Liu and Duan, 2014). Rupture propagation along connecting faults can facilitate jumping a larger distance across a stepover (Lozos et al, 2011). The length of a smaller disconnected intermediate fault between the main strands, and its basal depth, as well as whether the stepover is releasing or restraining, all contribute to the rupture behavior (Lozos, 2012; Lozos et al, 2015).

Our results of the long-term stress field around stepovers are also subjected to the influence of model parameters and boundary conditions (Wang et al., 2017). For example, viscosity contrast across a fault may produce asymmetrical stress localization along the fault, then cause abandonment of old faults and initiation of new faults around a stepover to accommodate crustal deformation more efficiently (Wakabayashi et al., 2004). Laterally variable gravitational potential energy, or basal shear, also affect the stress field around stepovers (Lynch and Richards, 2001). Fault dip could affect the vertical motion around stepovers (Smit et al., 2008; Choi et al., 2011).

Although the absolute values of stress variation in our long-term fault stress model vary with model parameters and boundary conditions, the basic physics of how releasing and restraining stepovers change the local stress field, and the spatial patterns of the stress change, are robust (Wang et al., 2017; Duan, 2019). To integrate these results into dynamic rupture models as perturbations to the initial stress, we normalized the steady-state stress variations, using the stress drop as the scaling factor to add long-term steady state stress perturbation to the homogenous initial stress in the dynamic rupture model. This process makes stress disturbances comparable among models with different fault geometry.

Implications for seismic hazard assessment

393

394

395

396

397

398

399

400

401

402

403

404

405

406

407

408

409

410

411

412

413

414

415

416

417

The potential rupture length along an active fault system is one of the most important inputs in seismic hazard assessment, because it controls the magnitude of an earthquake. Major earthquakes usually rupture multi-segments along a fault with several fault irregularities. So, the maximum jumping distance across stepovers is an important factor in seismic hazard assessment. One kind of general approach that is widely used in probabilistic seismic hazard analysis is the characteristic earthquake recurrence model (Giardini, 1999), which suggests that individual fault segments tend to generate characteristic earthquakes with nearly same size (Schwartz and Coppersmith, 1984). However, the 2011 Tohoku Mw 9.0 earthquake ruptured three fault segments where three individual magnitude-8 earthquakes could be allowed respectively (Geller, 2011). The complex spatiotemporal occurrence pattern of intraplate earthquakes also show limits of the characteristic earthquake recurrence model (Liu et al,. 2011). With a set of rupture rules, new cascade models considering multi-segment and complex multi-fault ruptures have been proposed. For example, in the Uniform California Earthquake Rupture Forecast, Version 3 (UCERF3), fault-to-fault jumping is allowed. In that model, fault segments separated less than 5 km are assumed to be connected. In extreme cases, a rupture can extend essentially anywhere in the whole San Andreas fault system with very low occurrence rates (Field et al., 2014, 2017; Schwartz, 2018). However, the small jumping distance across stepovers in UCERF3 may lead to an underestimate of the potential seismic hazard. Previous field observations show that ~10-12 km is the largest distance that a dip-slip earthquake rupture can break across a stepover (Biasi

and Wesnousky, 2016). Many devastating earthquakes in recent years ruptured multiple fault

segments, highlighting the pressing need to better understand the dynamics of fault rupture

over stepovers. Results from our simple models show that rupture can jump a very wide stepover if favorable conditions are met.

Conclusions

In this study, we incorporate changes of background stress around stepovers, derived from modeling long-term fault evolution, into models of dynamic fault rupture to systematically explore rupture propagation across stepovers on a strike-slip fault. Our models predict that fault rupture can jump over stepovers much wider than the 5-km limit previously thought: up to 20 km across overlapping releasing stepovers and 7 km across overlapping retraining stepovers.

A major reason for the predicted larger jumping distance across stepovers is the non-uniform initial stress. As a fault discontinuity, stepovers change the background stress around them, elevating compressive normal stress for restraining stepovers and extensional normal stress for releasing stepovers, and increasing shear stress for all stepovers. In most cases these non-uniform background stresses facilitate rupture propagation across the stepovers.

Fault geometry and frictional properties also have important impacts on the propagation of rupture across stepovers. An overlapping stepover is easier for rupture to jump than an underlapping stepover. The effects of frictional properties, including the static and dynamic frictional coefficients and the stress drop, can be collectively expressed by the S values. Lower S value favors rupture to jump over a wider stepover.

Data and Resources

No data were used in this paper. All plots were made using the Generic Mapping Tools version

5.4.2 (http://gmt.soest.hawaii.edu/; Wessel, 2013).

442

439

Acknowledgements

We are grateful to the Editor, Ruth Harris, and an anonymous reviewer for their constructive comments, which improved the manuscript. This work was mainly carried out during Wang's visit to the University of Missouri. Wang acknowledge support from National Natural Science Foundation of China (Grant 41774111, 41974111) and the China Scholarship Council (Grant 201704190035). Liu's work is supported by NSF grant 1519980. Duan acknowledges support from NSF through grant EAR-1524743.

452 References

463

464 465

466

472

473

474 475

476

- Andrews, D. J. (1976a). Rupture propagation with finite stress in antiplane strain, Journal of Geophysical Research-Solid Earth. 81, no.20, 3575-3582.
- Andrews, D. J. (1976b). Rupture velocity of plane strain shear cracks, Journal of Geophysical Research-Solid Earth. 81, no.32, 5679-5687.
- Andrews, D. J. (1985). Dynamic plane-strain shear rupture with a slip-weakening friction law calculated by a boundary integral method, Bulletin of the Seismological Society of America. 75, no.1, 1-21.
- 460 Aochi, H., R. Madariaga, and E. Fukuyama (2002). Effect of normal stress during rupture 461 propagation along nonplanar faults, Journal of Geophysical Research-Solid Earth. 107, 462 no.B2, ESE 5-1-ESE 5-10. doi:https://doi.org/10.1029/2001JB000500
 - Bai, K., and J.-P. Ampuero (2017). Effect of Seismogenic Depth and Background Stress on Physical Limits of Earthquake Rupture Across Fault Step Overs, Journal of Geophysical Research-Solid Earth. 122, no.12, 10280-10298. doi:10.1002/2017JB014848
- Biasi, G. P., and S. G. Wesnousky (2016). Steps and Gaps in Ground Ruptures: Empirical Bounds on Rupture Propagation, Bulletin of the Seismological Society of America. 106, no.3, 1110-1124. doi:10.1785/0120150175.
- Biasi, G. P., and S. G. Wesnousky (2017). Bends and Ends of Surface Ruptures, Bulletin of the Seismological Society of America. 107, no.6, 2543-2560. doi:10.1785/0120160292.
 - Byerlee, J. D. (1978). Friction of rocks, Pure and Applied Geophysics. 116, no.4-5, 615-626. doi:https://doi.org/10.1007/BF00876528.
 - Caniven, Y., S. Dominguez, R. Soliva, M. Peyreta, R. Cattina, and F. Maerten (2017). Relationships between along-fault heterogeneous normal stress and fault slip patterns during the seismic cycle: Insights from a strike-slip fault laboratory model, Earth and Planetary Science Letters. 480, 147-157. doi:10.1016/j.epsl.2017.10.009.
- Choi, E., L. Seeber, M. S. Steckler, and R. Buck (2011). One-sided transform basins and "inverted curtains": Implications for releasing bends along strike-slip faults, Tectonics. 30, no.TC6006. doi:10.1029/2011TC002943.
- Cooke, M. L., M. T. Schottenfeld, and S. W. Buchanan (2013). Evolution of fault efficiency at restraining bends within wet kaolin analog experiments, Journal of Structural Geology.
 51, 180-192. doi:10.1016/j.jsg.2013.01.010.
- Cunningham, W. D., and P. Mann (2007). Tectonics of strike-slip restraining and releasing bends, Geological Society, London, Special Publications. 290, 1-12. doi:10.1144/SP290.1.
- Das, S., and K. Aki (1977). A numerical study of two-dimensional spontaneous rupture propagation, Geophys. J. R. astr. Soc. 50, 643-668.
- Day, S. M. (1982). Three-dimentional simulation of spontaneous rupture: the effect of nonuniform prestress, Bulletin of the Seismological Society of America. 72, no.6, 1881-1902.
- Day, S. M., L. A. Dalguer, N. Lapusta, and Y. Liu (2005). Comparison of finite difference and boundary integral solutions to three-dimensional spontaneous rupture, Journal of Geophysical Research-Solid Earth. 110, no.B12. doi:10.1029/2005JB003813
- Dieterich, J. H., and K. B. Richards-Dinger (2010). Earthquake Recurrence in Simulated Fault Systems, Pure and Applied Geophysics. 167, 1087-1104. doi:10.1007/s00024-010-0094-0.
- Drucker, D. C., and W. Prager (1952). Soil mechanics and plastic analysis or limit design, Quarterly of applied mathematics. 10, no.2, 157-165.

- Duan, B. (2019). Multicycle Dynamics of the Aksay Bend Along the Altyn Tagh Fault in Northwest China: 1. A Simplified Double Bend, Tectonics. 38, no.3, 1101-1119. doi:https://doi.org/10.1029/2018TC005195.
- Duan, B., and S. M. Day (2008). Inelastic strain distribution and seismic radiation from rupture
 of a fault kink, Journal of Geophysical Research-Solid Earth. 113, no.B12311.
 doi:10.1029/2008JB005847.

507

508

511

512513

514

515

516

517

518519

520

521

522

523

524 525

526

529

530

531

532

533 534

535

536

537

- Duan, B., Z. Liu, and A. J. Elliott (2019). Multicycle Dynamics of the Aksay Bend Along the Altyn Tagh Fault in Northwest China: 2. The Realistically Complex Fault Geometry, Tectonics. 38, no.3, 1120-1137. doi:https://doi.org/10.1029/2018TC005196.
- Duan, B., and D. D. Oglesby (2005). Multicycle dynamics of nonplanar strike-slip faults, Journal of Geophysical Research. 110, no.B03304. doi:10.1029/2004JB003298.
 - Duan, B., and D. D. Oglesby (2006). Heterogeneous fault stresses from previous earthquakes and the effect on dynamics of parallel strike-slip faults, Journal of Geophysical Research. 111, no.B05309, doi:10.1029/2005JB004138.
 - Field, E. H., R. J. Arrowsmith, G. P. Biasi, P. Bird, T. E. Dawson, K. R. Felzer, D. D. Jackson, K. M. Johnson, T. H. Jordan, C. Madden, A. J.Michael, K. R. Milner, M. T. Page, T. Parsons, P. M. Powers, B. E. Shaw, W. R. Thatcher, R. J. W. II, and Y. Zeng (2014). Uniform California Earthquake Rupture Forecast, Version 3 (UCERF3)-The Time-Independent Model, Bulletin of the Seismological Society of America. 104, no.3, 1122-1180. doi:10.1785/0120130164.
 - Field, E. H., T. H. Jordan, M. T. Page, K. R. Milner, B. E. Shaw, T. E. Dawson, G. P. Biasi, T. Parsons, J. L. Hardebeck, A. J. Michael, R. J. Weldon, P. M. Powers, K. M. Johnson, Y. Zeng, K. R. Felzer, N. v. d. Elst, C. Madden, R. Arrowsmith, M. J. Werner, and W. R. Thatcher (2017). A Synoptic View of the Third Uniform California Earthquake Rupture Forecast (UCERF3), seismological research letters. 88, no.5, 1259-1267. doi:10.1785/0220170045.
 - Geller, R. J. (2011). Shake-up time for Japanese seismology, Nature. 472, 407-409.
- Giardini, D., G. Grunthal, K. M. Shedlock, and P. Zhang (1999). The GSHAP Global Seismic
 Hazrd Map, ANNALI DI GEOFISICA. 42, no.6, 1225-1230.
 - Hamling, I. J., S. Hreinsdóttir, K. Clark, J. Elliott, C. Liang, E. Fielding, N. Litchfield, P. Villamor, L. Wallace, T. J. Wright, E. D'Anastasio, S. Bannister, D. Burbidge, P. Denys, P. Gentle, J. Howarth, C. Mueller, N. Palmer, C. Pearson, W. Power, P. Barnes, D. J. A. Barrell, R. V. Dissen, R. Langridge, T. Little, A. Nicol, J. Pettinga, J. Rowland, and M. Stirling (2017). Complex multifault rupture during the 2016 Mw 7.8 Kaikōura earthquake, New Zealand, Science. 356, no.6334. doi:10.1126/science.aam7194.
 - Harris, R. A., R. J. Archuleta, and S. M. Day (1991). Fault steps and the dynamic rupture process: 2-D numerical simulations of a spontaneously propagating shear fracture, Geophysical Research Letters. 18, no.5, 893-896. doi:https://doi.org/10.1029/91GL01061.
- Harris, R. A., M. Barall, B. Aagaard, S. Ma, D. Roten, K. Olsen, B. Duan, D. Liu, B. Luo, K.
 Bai, J. P. Ampuero, Y. Kaneko, A. A. Gabriel, K. Duru, T. Ulrich, S. Wollherr, Z. Shi,
 E. Dunham, S. Bydlon, Z. Zhang, X. Chen, S. N. Somala, C. Pelties, J. Tago, V. M.
 Cruz-Atienza, J. Kozdon, E. Daub, K. Aslam, Y. Kase, K. Withers, and L. Dalguer
 (2018). A Suite of Exercises for Verifying Dynamic Earthquake Rupture Codes,
 seismological research letters. 89, no.3, 1146-1162. doi:10.1785/0220170222.
- Harris, R. A., M. Barall, D. J. Andrews, B. Duan, S. Ma, E. M. Dunham, A.-A. Gabriel, Y. 545 Kaneko, Y. Kase, B. T. Aagaard, D. D. Oglesby, J.-P. Ampuero, T. C. Hanks, and N. 546 547 Abrahamson (2011). Verifying a Computational Method for Predicting Extreme 548 Ground Motion. seismological research letters. 82, no.5, 638-644. doi:10.1785/gssrl.82.5.638. 549

- Harris, R. A., M. Barall, R. Archuleta, E. Dunham, B. Aagaard, J. P. Ampuero, H. Bhat, B.
 Duan, G. Ely, Y. Kaneko, Y. Kase, N. Lapusta, Y. Liu, S. Ma, D. Oglesby, K. Olsen,
 A. Pitarka, S. Song, and E. Tempeton (2009). The SCEC/USGS dynamic earthquake
 rupture code verification exercise, seismological research letters. 80, no.1, 119-126.
 doi:10.1785/gssrl.80.1.119.
- Harris, R. A., and S. M. Day (1993). Dynamics of fault interaction: Parallel strike-slip faults, Journal of Geophysical Research-Solid Earth. 98, no.B3, 4461-4472.
- Harris, R. A., and S. M. Day (1999). Dynamic 3-D simulations of earthquakes on en echelon faults, Geophysical Research Letters. 26, no.14, 2089-2092. doi:https://doi.org/10.1029/1999GL900377
- Hatem, A. E., M. L. Cooke, and E. H. Madden (2015). Evolving efficiency of restraining bends
 within wet kaolin analog experiments, Journal of Geophysical Research-Solid Earth.
 120, no.3, 1975-1992. doi:10.1002/2014JB0011735.
- Hu, F., Z. Zhang, and X. Chen (2016). Investigation of earthquake jump distance for strikeslip step overs based on 3-D dynamic rupture simulations in an elastic half-space, Journal of Geophysical Research-Solid Earth. 121, no.2, 994-1006. doi:10.1002/2015JB012696.

568 569

570

571572

575

576

577578

582

- Kaiser, A., N. Balfour, B. Fry, C. Holden, N. Litchfield, M. Gerstenberger, E. D'Anastasio, N. Horspool, G. McVerry, J. Ristau, S. Bannister, A. Christophersen, K. Clark, W. Power, D. Rhoades, C. Massey, I. Hamling, L. Wallace, J. Mountjoy, Y. Kaneko, R. Benites, C. V. Houtte, S. Dellow, L. Wotherspoon, K. Elwood, and K. Gledhill (2017). The 2016 Kaikōura, New Zealand, Earthquake: Preliminary Seismological Report, seismological research letters. 88, no.3, 727-739. doi:10.1785/0220170018.
- Kase, Y., and K. Kuge (2001). Rupture propagation beyond fault discontinuities: significance of fault strike and location, Geophysical Journal International. 147, 330-342.
 - Kijko, A., and M. A. Sellevoll (1989). Estimation of earthquake hazard parameters from incomplete data files. Part I. Utilization of extreme and complete catalogs with different threshold magnitudes, Bulletin of the Seismological Society of America. 79, no.3, 645-654.
- Li, Q., and M. Liu (2006). Geometrical impact of the San Andreas Fault on stress and seismicity in California, Geophysical Research Letters. 33, no.L08302, doi:10.1029/2005GL025661.
 - Li, Q., M. Liu, and H. Zhang (2009). A 3-D viscoelastoplastic model for simulating long-term slip on non-planar faults, Geophysical Journal International. 176, 293-306, doi:10.1111/j.1365-246X.2008.03962.x.
- Liu, M., S. Stein, and H. Wang (2011). 2000 years of migrating earthquakes in North China: how earthquakes in mid-continents differ from thoese at plate boundaires, Lithosphere. 3, no.2, 128-132. doi:10.1130/L129.1.
- Liu, M., H. Wang, and Q. Li (2010). Inception of the Eastern California Shear Zone and evolution of the Pacific-North American plate boundary: From kinematics to geodynamics, Journal of Geophysical Research-Solid Earth. 115, no.B07401. doi:10.1029/2009JB007055.
- Liu, Z., and B. Duan (2014). Dynamics of parallel strike-slip faults with pore fluid pressure change and off-fault damage, Bulletin of the Seismological Society of America. 104, no.2, 780-792. doi:10.1785/0120130112.
- 595 Liu, Z., and B. Duan (2015). Coseismic Slip Gradient and Rupture Jumps on Parallel Strike-596 Slip Faults, Bulletin of the Seismological Society of America. 106, no.1, 204-212. 597 doi:10.1785/0120140337.
- Lozos, J. C. (2016). A case for historic joint rupture of the San Andreas and San Jacinto faults, Science Advances. 2, no.3, e1500621. doi:10.1126/sciadv.1500621.

- Lozos, J. C., J. H. Dieterich, and D. D. Oglesby (2014). The effects of d0 on rupture propagation on fault stepover, Bulletin of the Seismological Society of America. 104, no.4, 1947-1953. doi:10.1785/0120130305.
- Lozos, J. C., R. A. Harris, J. R. Murray, and J. J. Lienkaemper (2015a). Dynamic rupture models of earthquakes on the Bartlett Springs Fault, Northern California, Geophysical Research Letters. 42, no.11, 4343-4349. doi:10.1002/2015GL063802.
- 606 Lozos, J. C., D. D. Oglesby, J. N. Brune, and K. B. Olsen (2012). Small intermediate fault 607 segments can either aid or hinder rupture propagation at stepovers, Geophysical 608 Research Letters. 39, no.L18305. doi:10.1029/2012GL053005.
- Lozos, J. C., D. D. Oglesby, J. N. Brune, and K. B. Olsen (2015b). Rupture propagation and ground motion of strike-slip stepover with intermediate fault segement, Bulletin of the Seismological Society of America. 105, no.1, 387-399. doi:10.1785/0120140114.
- Lozos, J. C., D. D. Oglesby, B. Duan, and S. G. Wesnousky (2011). The effects of double fault bends on rupture propagation: A Geometrical parameter study, Bulletin of the Seismological Society of America. 101, no.1, 385-398. doi:10.1785/0120100029.
- Luo, B., and B. Duan (2018). Dynamics of Nonplanar Thrust Faults Governed by Various Friction Laws, Journal of Geophysical Research-Solid Earth. 123, no.6, 5147-5168. doi:10.1029/2017JB015320.
- Lynch, J. C., and M. A. Richards (2001). Finite element models of stress orientations in well-developed strike-slip fault zones: Implications for the distribution of lower crustal strain,
 Journal of Geophysical Research-Solid Earth. 106, no.B11, 26707-26729.
- Mann, P. (2007). Global catalogue, classification and tectonic origins of restraining- and releasing bends on active and ancient strike-slip fault systems, Geological Society, London, Special Publications. 290, 13-142. doi:10.1144/SP290.2.
- 624 McClay, K., and M. Bonora (2001). Analog models of restraining stepovers in strike-slip fault 625 systems, AAPG Bulletin. 85, no.2, 233-260. doi:10.1306/8626C7AD-173B-11D7-626 8645000102C1865D.
- Micklethwaite, S., A. Ford, W. Witt, and H. A. Sheldon (2015). The where and how of faults, fluids and permeability insights from fault stepovers, scaling properties and gold mineralisation, Geofluids. 15, 240-251. doi:10.1111/gfl.12102.
- Oglesby, D. (2008). Rupture Termination and Jump on Parallel Offset Faults, Bulletin of the Seismological Society of America. 98, no.1, 440-447. doi:https://doi.org/10.1785/0120070163.
- Oglesby, D. D. (2005). The Dynamics of Strike-Slip Step-Overs with Linking Dip-Slip Faults,
 Bulletin of the Seismological Society of America. 95, no.5, 1604-1622.
 doi:10.1785/0120050058.
- Olsen, K. B., R. Madariaga, and R. J. Archuleta (1997). Three-Dimensional Dynamic Simulation of the 1992 Landers Earthquake, Science. 278, 834-838. doi:10.1126/science.278.5339.834.
- Ryan, K. J., and D. D. Oglesby (2014). Dynamically modeling fault step overs using various friction laws, Journal of Geophysical Research-Solid Earth. 119, no.7, 5814-5829. doi:10.1002/2014JB011151
- 642 Schwartz, D. P. (2018). Past and Future Fault Rupture Lengths in Seismic Source 643 Characterization—The Long and Short of It, Bulletin of the Seismological Society of 644 America. 108, no.5A, 2493-2520. doi:10.1785/0120160110.
- Schwartz, D. P., and K. J. Coppersmith (1984). Fault Behavior and Characteristic Earthquakes:
 Examples From the Wasatch and San Andreas Fault Zones, Journal of Geophysical
 Research-Solid Earth. 89, no.B7, 5681-5698.
- Scognamiglio, L., E. Tinti, E. Casarotti, S. Pucci, F. Villani, M. Cocco, F. Magnoni, A.
 Michelini, and D. Dreger (2018). Complex Fault Geometry and Rupture Dynamics of

- the MW 6.5, 30 October 2016, Central Italy Earthquake, Journal of Geophysical Research-Solid Earth. 123, no.4, 2943-2964. doi:10.1002/2018JB015603.
- Shao, Y., J. Liu-Zeng, M. E. Oskin, A. J. Elliott, P. Wang, J. Zhang, Z. Yuan, and Z. Li (2018).
 Paleoseismic Investigation of the Aksay Restraining Double Bend, Altyn Tagh Fault,
 and Its Implication for Barrier-Breaching Ruptures, Journal of Geophysical Research Solid Earth. 123, no.5, 4307-4330. doi:10.1029/2017JB015397

- Sibson, R. H. (1985). Stopping of earthquake ruptures at dilational fault jogs, Nature. 316, 248-251. doi:10.1038/316248a0.
- Smit, J., J.-P. Brun, S. Cloetingh, and Z. Ben-Avraham (2008). Pull-apart basin formation and development in narrow transform zones with application to the Dead Sea Basin, Tectonics. 27, no.TC6018. doi:10.1029/2007TC002119.
- Sylvester, A. G. (1988). Strike-slip faults, Geological Society of America Bulletin. 100, no.11, 1666-1703. doi:10.1130/0016-7606(1988)100<1666:ssf>2.3.co;2.
- Ulrich, T., A.-A. Gabriel, J.-P. Ampuero, and W. Xu (2019). Dynamic viability of the 2016 Mw 7.8 Kaikōura earthquake cascade on weak crustal faults, Nature Communications. 10, no.1213. doi:https://doi.org/10.1038/s41467-019-09125-w.
- Wakabayashi, J., J. V. Hengesh, and T. L. Sawyer (2004). Four-dimensional transform fault processes: progressive evolution of step-overs and bend, Tectonophysics. 392, 279-301. doi:10.1016/j.tecto.2004.04.013.
- Wald, D. J., and T. H. Heaton (1994). Spatial and temporal distribution of slip for the 1992 Landers, California, earthquake Bulletin of the Seismological Society of America. 84, no.3, 668-691.
- Wang, H., M. Liu, J. Ye, J. Cao, and Y. Jing (2017). Strain partitioning and stress perturbation around stepovers and bends of strike-slip faults: Numerical results, Tectonophysics. 721, no.28, 211-226. doi:10.1016/j.tecto.2017.10.001.
- Wesnousky, S. G. (2006). Predicting the endpoints of earthquake ruptures, Nature. 444, 358-360. doi:10.1038/nature05275.
 - Wesnousky, S. G. (2008). Displacement and Geometrical Characteristics of Earthquake Surface Ruptures: Issues and Implications for Seismic-Hazard Analysis and the Process of Earthquake Rupture, Bulletin of the Seismological Society of America. 98, no.4, 1609-1632. doi:10.1785/0120070111.
- Wijk, J. v., G. Axen, and R. Abera (2017). Initiation, evolution and extinction of pull-apart basins: Implications for opening of the Gulf of California, Tectonophysics. 719-720, 37-50. doi:10.1016/j.tecto.2017.04.019.
- Xu, X., W. Chen, W. Ma, G. Yu, and G. Chen (2002). Surface rupture of the Kunlunshan
 earthquake (Ms 8.1), northern Tibetan plateau, China, seismological research letters.
 73, no.6, 884-892.
- Ye, J., and M. Liu (2017). How fault evolution changes strain partitioning and fault slip rates in southern California: Results from geodynamic modeling, Journal of Geophysical Research-Solid Earth. 122, no.8, 6893-6909. doi:10.1002/2017JB014325.
- Ye, J., M. Liu, and H. Wang (2015). A numerical study of strike-slip bend formation with application to the Salton Sea pull-apart basin, Geophysical Research Letters. 42. doi:10.1002/2015GL063180.

695 Tables

Table 1Parameters of the three-dimensional viscoelastoplastic model

	Young's modulus	Poisson	Viscosity	Cohesion	Effective frictional
	(Pa)	Ratio	(Pa s)	(MPa)	coefficient
Upper Crust	8.75×10 ¹⁰	0.25	1.0×10 ²⁵	50	0.4
Lower crust and upper mantle	8.75×10 ¹⁰	0.25	2.0×10 ²⁰	50	0.4
Faults	8.75×10 ¹⁰	0.25	2.0×10 ²⁰	10	0.0-0.1

700 Table 2701 Major parameters in the reference dynamic rupture model

6,000 m/s		
6,000 m/s		
3,464 m/s		
$2,700 \text{ km/m}^3$		
0.75		
0.30		
0.50		
0.4 m		
-33.3 MPa		
$\pm20.0~\mathrm{MPa}$		
50 m		
1500 m		
0.05 s		
20.0 s		

704 Table 3705 Descriptions of different cases of dynamic rupture models

Cases	Homogenous stress	Stress perturbation around stepovers $(\Delta \sigma_{max})^*$	Over-/underlapping (Offset angles α)	Stress drop (Δτ)	Frictional coefficients
1 (ref.)	σ_0 =-33.3 MPa τ_0 =±20.0 MPa	0	overlapping	10 MPa	$\mu_s = 0.75$ $\mu_d = 0.30$
2	-	5.0 MPa 10.0 MPa	-	-	-
3	-	-	Underlapping α=90°, 105°, 120°, 135°, 150°, 165°	-	-
4	-	5.0 MPa 10.0 MPa	Underlapping α =150°, 165°	-	-
5	-	-	Over- and underlapping	-	$\mu_s = 0.65$
6	-	-	Over- and underlapping (α=150°)	3-11 MPa	Varying μ _d

^{*} $\Delta\sigma_{max}$ is the maximum variation of stress perturbation based on long-term steady state stress modeling and stress drop on

fault segments. Dash means the same as in the reference case.

List of Figure Captions

Figure 1. The mechanical model of a strike-slip fault offset by a stepover. (a) Numerical mesh and boundary conditions of the 3D finite element model for simulating long-term stress variations around the stepover. The black lines are strike-slip faults. The upper layer (light grey) represents the brittle (elastoplastic) upper crust; the lower layer (dark grey) represents the viscoplastic lower crust and upper mantle. Long black line with the shorter lines show the model is fixed on the back side. The arrows show velocity loading on the front side. (b) Enlargement of the area (Box in (a)) around the stepover that is used in the 2D model of rupture propagation. Two parallel faults have the same length of 28.0 km, and the overlap is 5.0 km. In each case (Table 3), the stepover width (W) is incrementally increased until the rupture is arrested by the stepover. (c) Enlargement of the area (Box in (b)) to show the fault geometric parameters: the width of the stepover (W) and the offset angle α that indicating overlapping (α < 90°) or underlapping (α > 90°).

Figure 2. Long-term steady-state stress perturbation around a simple stepover, all in map view for the surficial values. (a) σ_{yy} around a releasing stepover; (b) σ_{yy} around a restraining stepover; (c) σ_{xy} around a releasing stepover; (d) σ_{xy} around a restraining stepover. The color version of this figure is available only in the electronic edition.

Figure 3. Long-term steady-state stress perturbation on the fault plane of the left fault segment of the stepovers. (a) normal stress of a releasing stepover; (b) normal stress of a restraining stepover; (c) shear stress of a releasing stepover; (d) shear stress of a restraining stepover. The color version of this figure is available only in the electronic edition.

Figure 4. Initial yield stress (solid curves) and shear stress (dash curves) for the dynamic rupture model for a releasing stepover (a) and restraining stepover (b). Black thick curves are the yield and shear stresses on the left fault segment, gray thick curves are for the right fault segment. Thin curves are the yield stress and shear stresses for a reference case of homogeneous initial stress on the fault segments.

Figure 5. Snapshot of stress evolution and rupture propagation along fault segments of a releasing stepover (1-km width) at different times. Solid curves are yield stress, dash curves are shear stress, black curves are stress on the left fault segment, and gray curves are stress on the right fault segment.

Figure 6. Spatiotemporal evolution of slip along fault segments for the reference models of a releasing stepover (a) and restraining stepover (b). The two lines below the plots indicate the fault segments in map view. The color version of this figure is available only in the electronic edition.

Figure 7. Summary of modeled rupture behavior over stepovers with various width. Each line on the right side represents the right fault segment in one case, where together with the left fault segment they make a stepover. Positive width indicated releasing stepover, and negative width indicated restraining stepover. The crosses show where initial rupture on the right fault segment is triggered, and the time when rupture on the right fault segment is triggered is indicated on each fault. Black lines represent releasing stepover. Gray lines represent restraining stepover.

Figure 8. Summary of rupture behaviors in stepovers with varying width in models with a variable initial stress field around the stepover. The left line is the left fault segment; each line on the right side represents the right fault segment of across a stepover. The color of these lines indicates the S value at each fault node. Positive width indicated releasing stepover, and negative width indicated restraining stepover; Crosses represent the initial positions of rupture on the right fault. The maximum perturbation of the initial stress is 5 MPa (a) and 10 MPa (b), respectively. The color version of this figure is available only in the electronic edition.

Figure 9. Summary of the jumping distance across an underlapping stepover with homogenous initial stresses. The offset angle α indicate the degree of underlapping (see Figure. 1c). Crosses indicate the cases that rupture jumped over a restraining stepover with the specified stepover width and offset angle. Cycles indicate the cases for releasing stepovers.

Figure 10. Rupture behaviors on stepovers with a lower static friction coefficient (μ_s =0.65) in models with a homogenous initial stress field. (a) Overlapping stepovers. The lines and symbols are explained in Figure 7. Black lines represent releasing stepovers. Gray lines represent restraining stepovers. (b) Results for underlapping stepovers with varies widths and offset angles. See explanations in Figure 9.

Figure 11. Rupture behaviors on stepovers with varying stress drop in models with a homogenous initial stress field. (a) Results for overlapping stepovers (overlapping configurations are shown in Figure 7). Symbols are explained in Figure 7. (b) Results for underlapping stepovers, with an offset angle of α =150°.

785 Figures

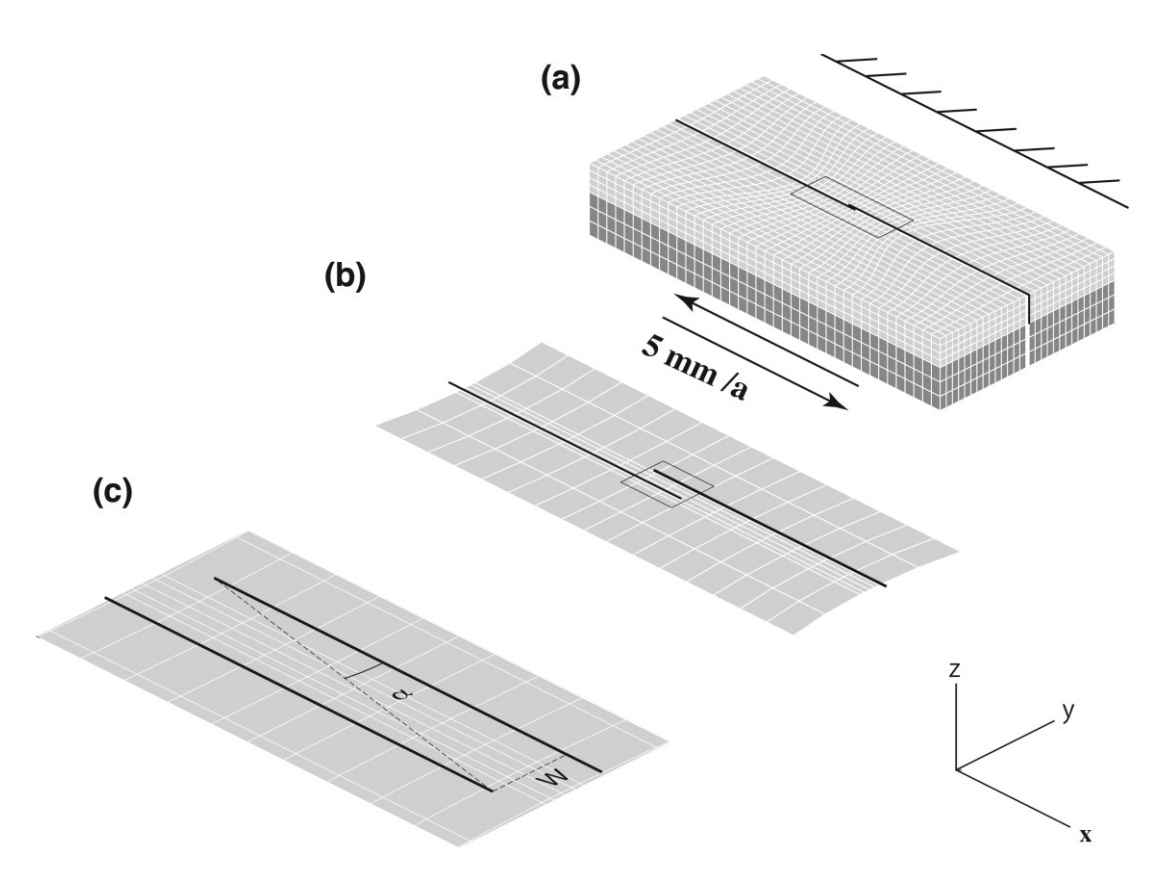


Figure 1. The mechanical model of a strike-slip fault offset by a stepover. (a) Numerical mesh and boundary conditions of the 3D finite element model for simulating long-term stress variations around the stepover. The black lines are strike-slip faults. The upper layer (light grey) represents the brittle (elastoplastic) upper crust; the lower layer (dark grey) represents the viscoplastic lower crust and upper mantle. Long black line with the shorter lines show the model is fixed on the back side. The arrows show velocity loading on the front side. (b) Enlargement of the area (Box in (a)) around the stepover that is used in the 2D model of rupture propagation. Two parallel faults have the same length of 28.0 km, and the overlap is 5.0 km. In each case (Table 3), the stepover width (W) is incrementally increased until the rupture is arrested by the stepover. (c) Enlargement of the area (Box in (b)) to show the fault geometric parameters: the width of the stepover (W) and the offset angle α that indicating overlapping ($\alpha < 90^{\circ}$) or underlapping ($\alpha > 90^{\circ}$).

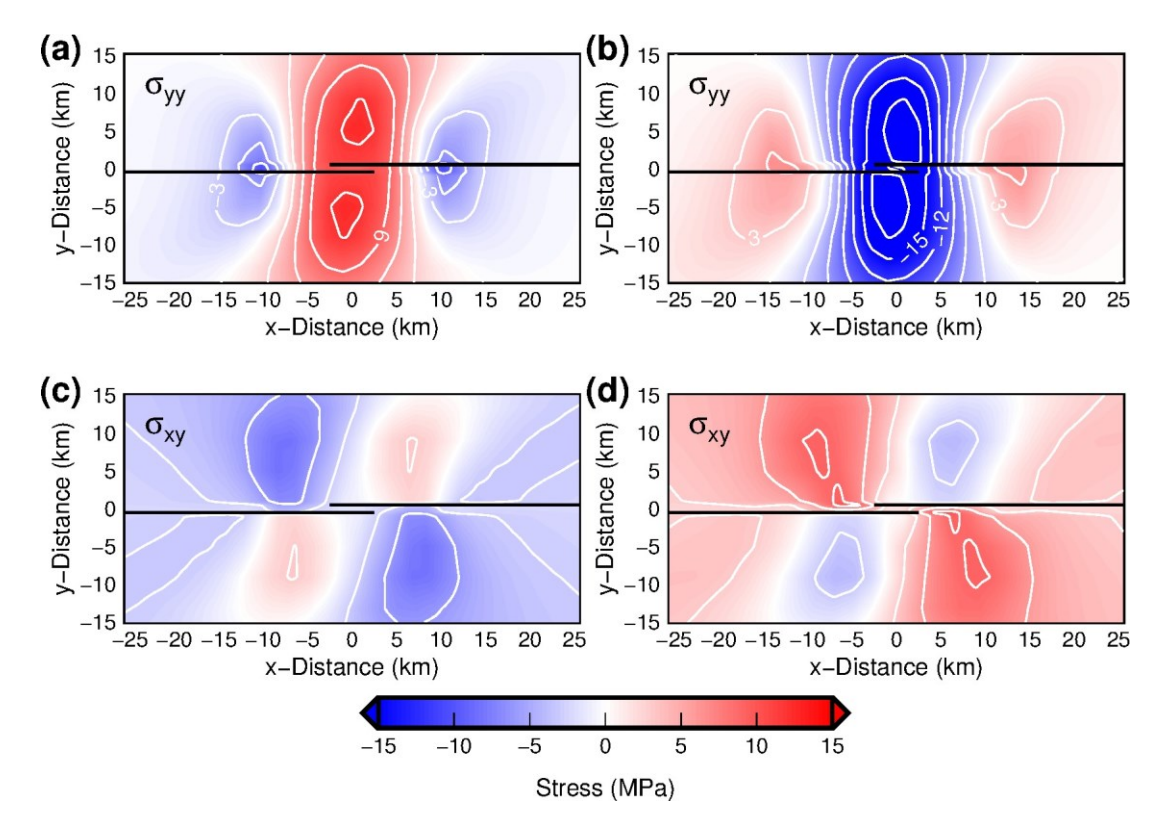


Figure 2. Long-term steady-state stress perturbation around a simple stepover, all in map view for the surficial values. (a) σ_{yy} around a releasing stepover; (b) σ_{yy} around a restraining stepover; (c) σ_{xy} around a releasing stepover; (d) σ_{xy} around a restraining stepover. The color version of this figure is available only in the electronic edition.

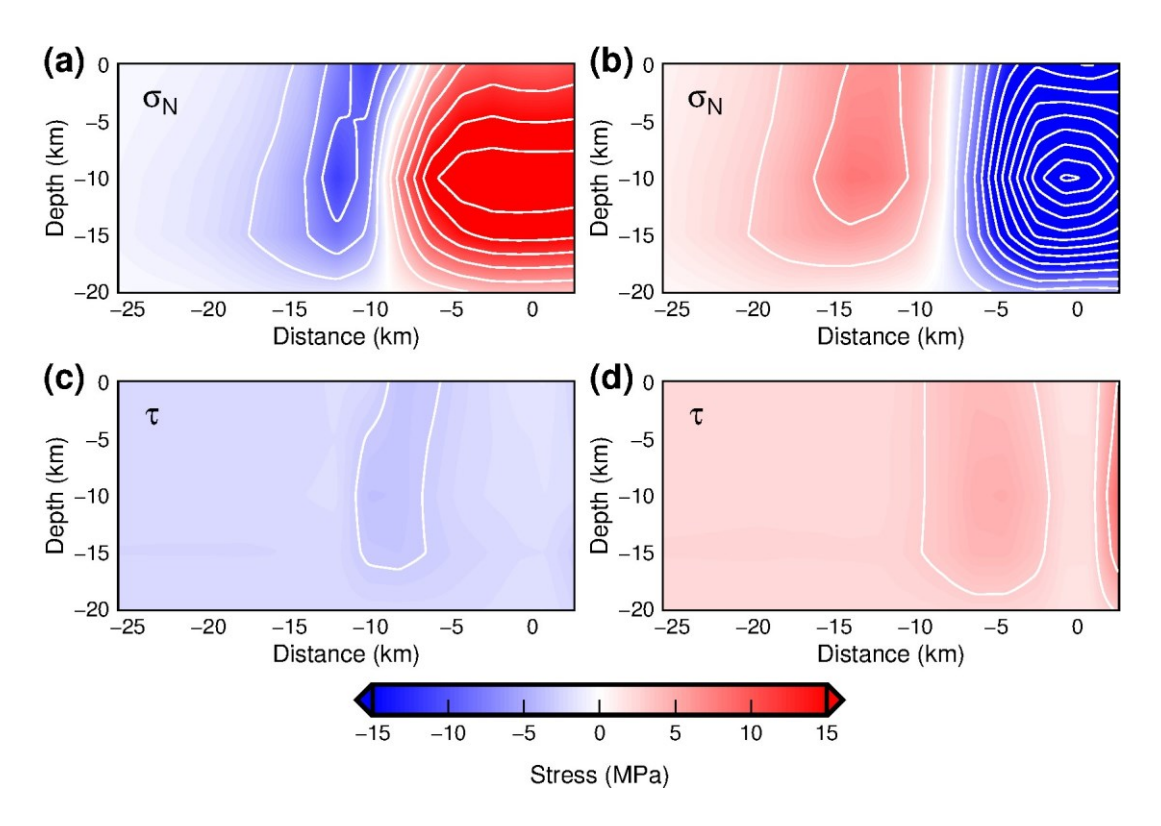


Figure 3. Long-term steady-state stress perturbation on the fault plane of the left fault segment of the stepovers. (a) normal stress of a releasing stepover; (b) normal stress of a restraining stepover; (c) shear stress of a releasing stepover; (d) shear stress of a restraining stepover. The color version of this figure is available only in the electronic edition.

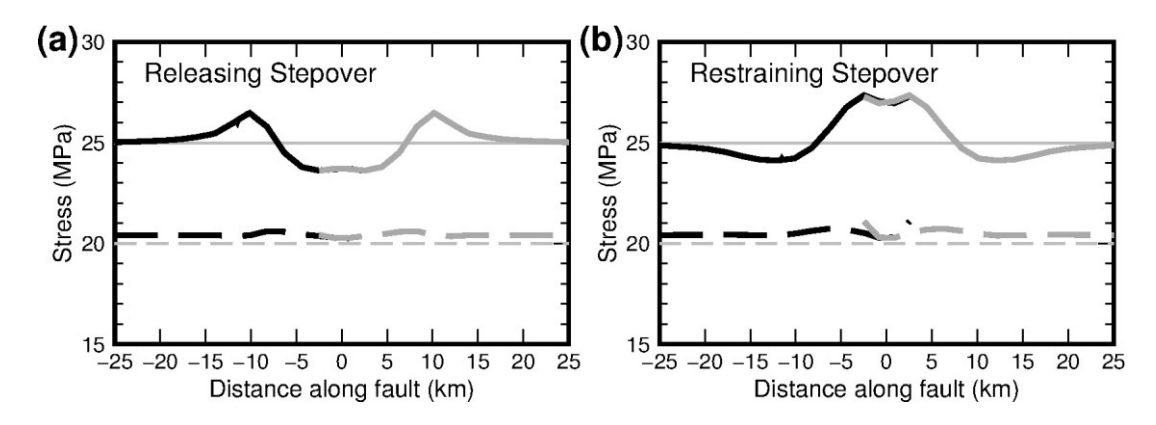


Figure 4. Initial yield stress (solid curves) and shear stress (dash curves) for the dynamic rupture model for a releasing stepover (a) and restraining stepover (b). Black thick curves are the yield and shear stresses on the left fault segment, gray thick curves are for the right fault segment. Thin curves are the yield stress and shear stresses for a reference case of homogeneous initial stress on the fault segments.

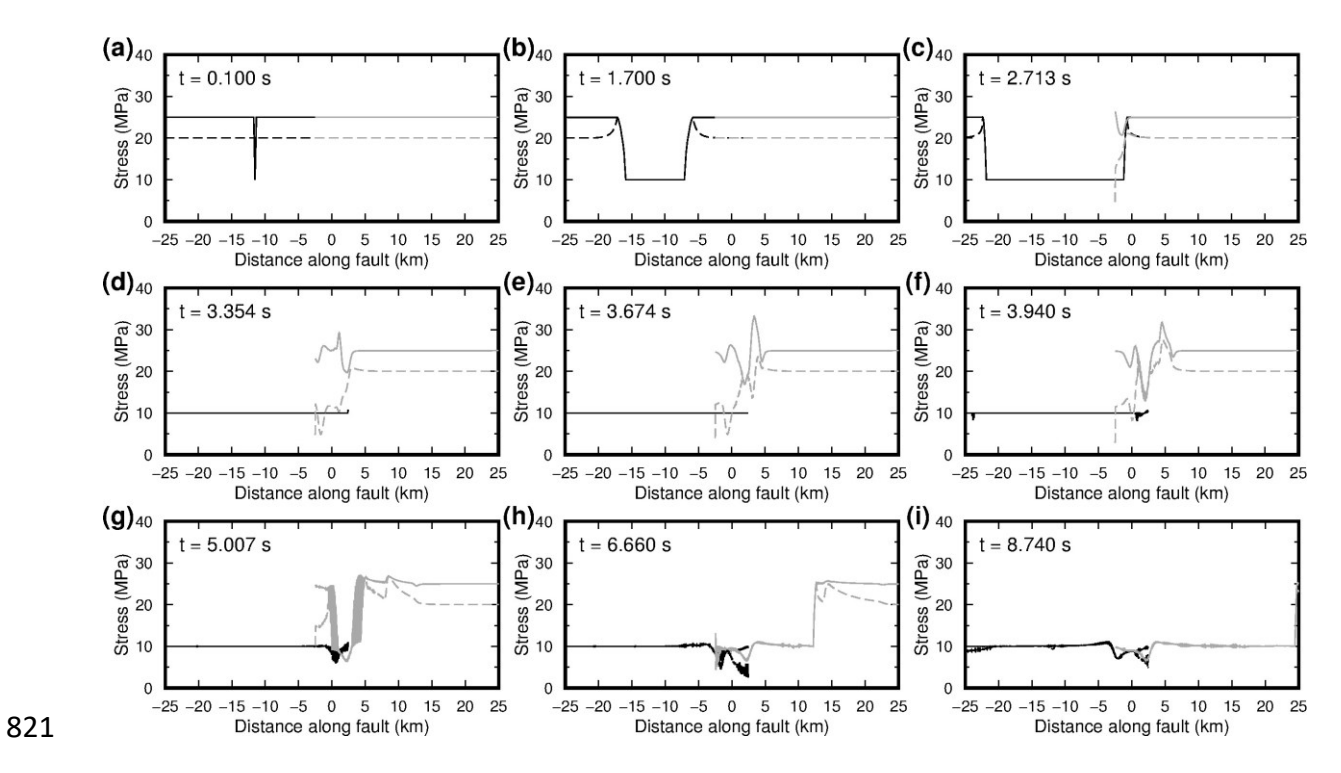


Figure 5. Snapshot of stress evolution and rupture propagation along fault segments of a releasing stepover (1-km width) at different times. Solid curves are yield stress, dash curves are shear stress, black curves are stress on the left fault segment, and gray curves are stress on the right fault segment.

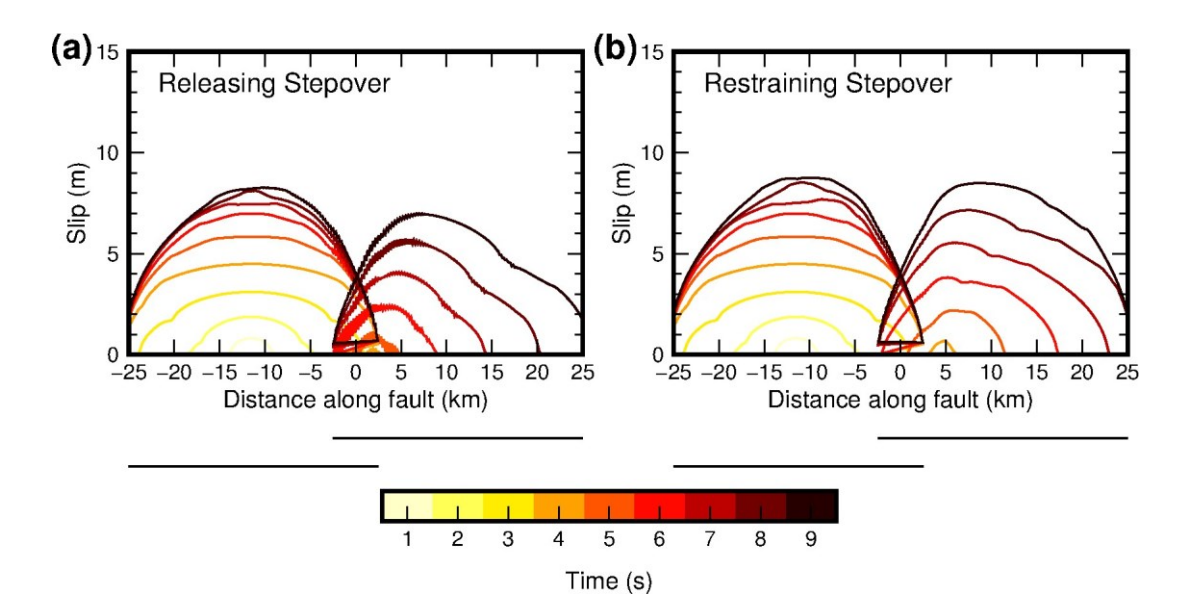


Figure 6. Spatiotemporal evolution of slip along fault segments for the reference models of a releasing stepover (a) and restraining stepover (b). The two lines below the plots indicate the fault segments in map view. The color version of this figure is available only in the electronic edition.

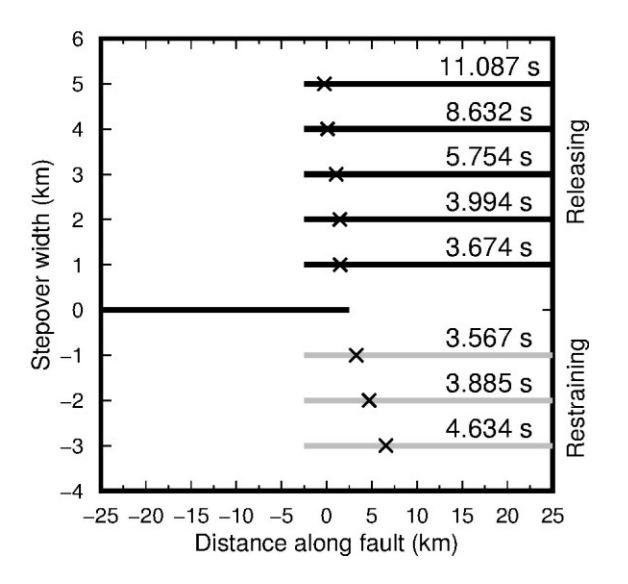


Figure 7. Summary of modeled rupture behavior over stepovers with various width. Each line on the right side represents the right fault segment in one case, where together with the left fault segment they make a stepover. Positive width indicated releasing stepover, and negative width indicated restraining stepover. The crosses show where initial rupture on the right fault segment is triggered, and the time when rupture on the right fault segment is triggered is indicated on each fault. Black lines represent releasing stepover. Gray lines represent restraining stepover.



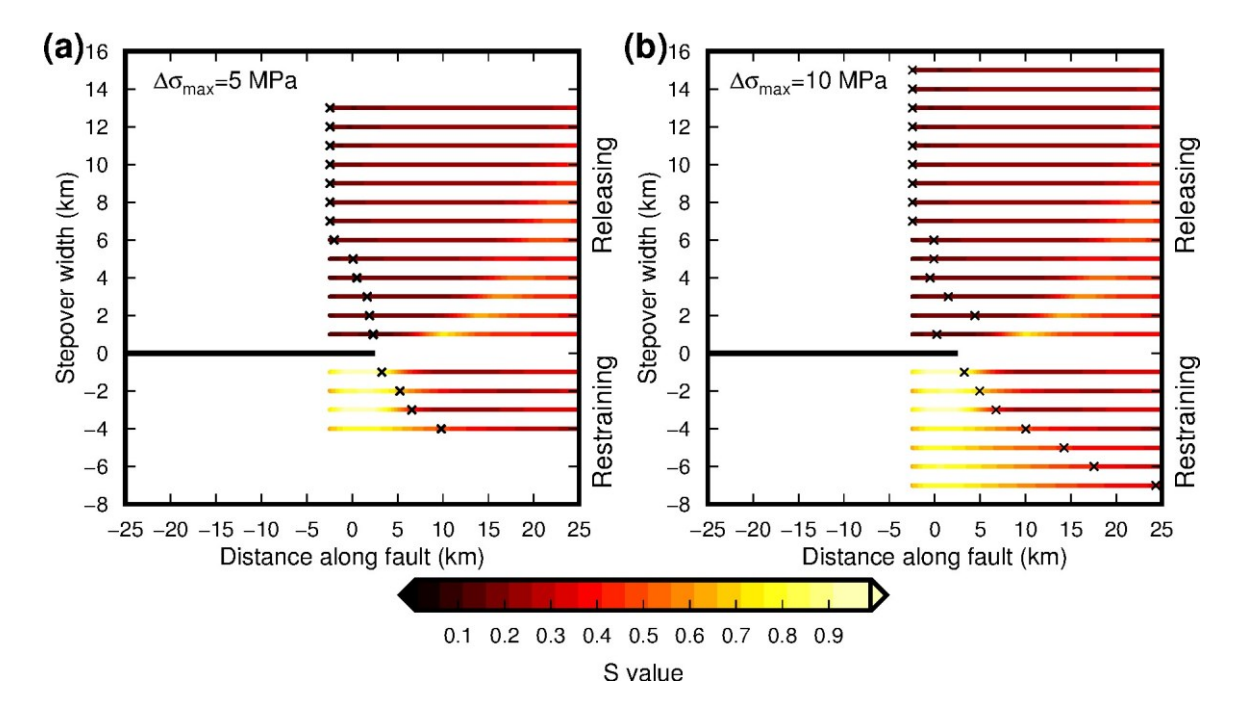


Figure 8. Summary of rupture behaviors in stepovers with varying width in models with a variable initial stress field around the stepover. The left line is the left fault segment; each line on the right side represents the right fault segment of across a stepover. The color of these lines indicates the S value at each fault node. Positive width indicated releasing stepover, and negative width indicated restraining stepover; Crosses represent the initial positions of rupture on the right fault. The maximum perturbation of the initial stress is 5 MPa (a) and 10 MPa (b), respectively. The color version of this figure is available only in the electronic edition.

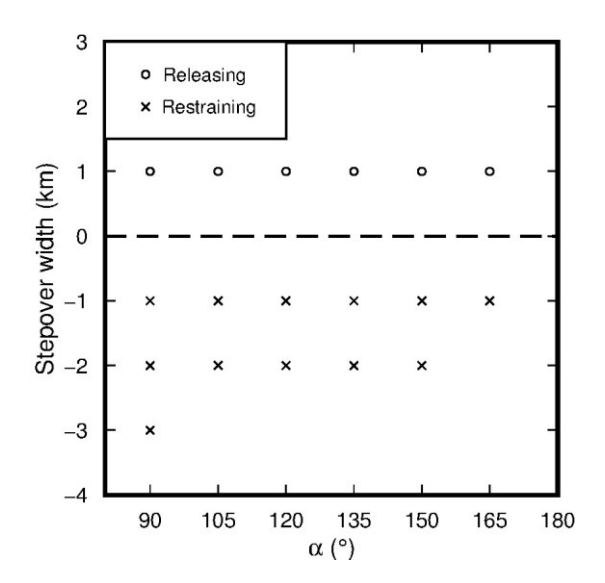


Figure 9. Summary of the jumping distance across an underlapping stepover with homogenous initial stresses. The offset angle α indicate the degree of underlapping (see Figure. 1c). Crosses indicate the cases that rupture jumped over a restraining stepover with the specified stepover width and offset angle. Cycles indicate the cases for releasing stepovers.

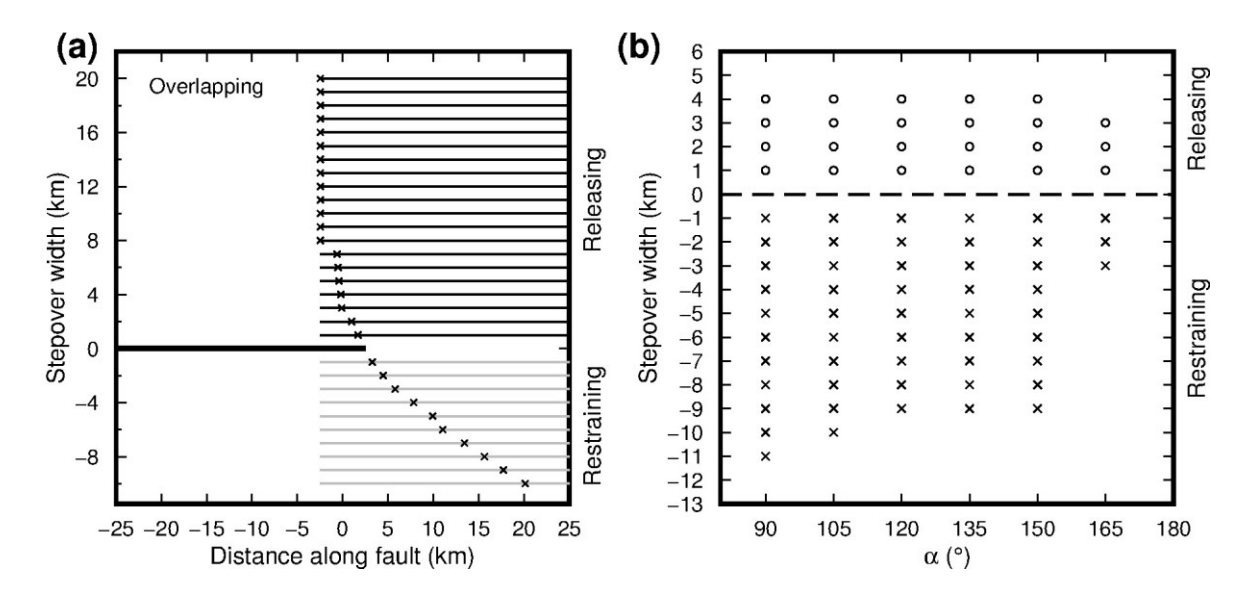


Figure 10. Rupture behaviors on stepovers with a lower static friction coefficient (μ_s =0.65) in models with a homogenous initial stress field. (a) Overlapping stepovers. The lines and symbols are explained in Figure 7. Black lines represent releasing stepovers. Gray lines represent restraining stepovers. (b) Results for underlapping stepovers with varies widths and offset angles. See explanations in Figure 9.



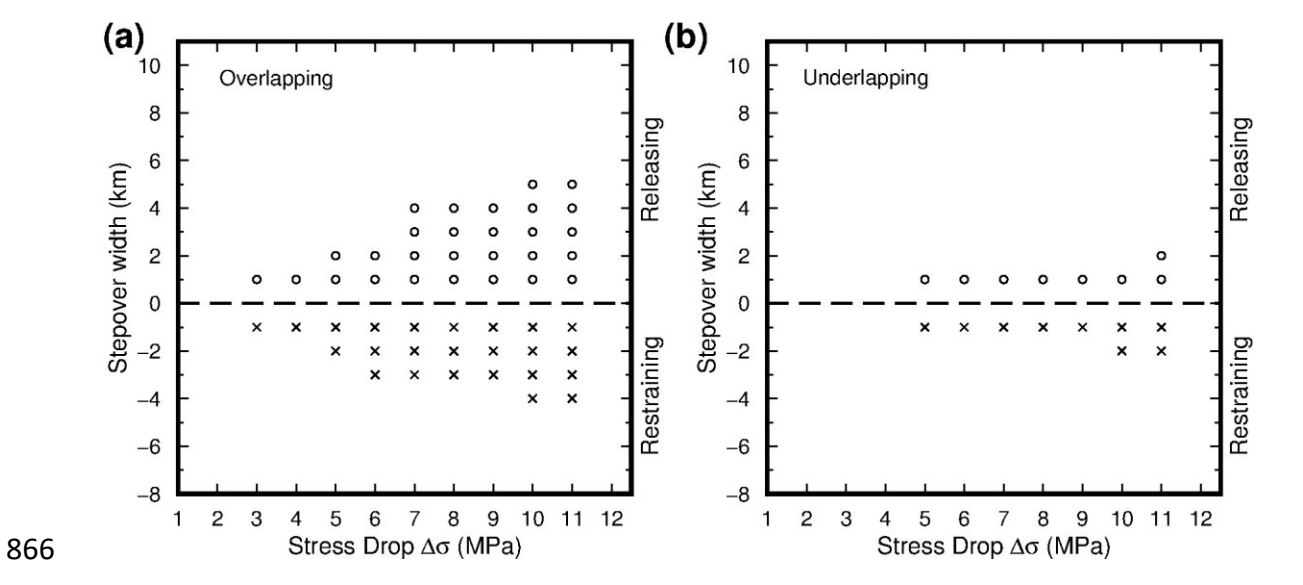


Figure 11. Rupture behaviors on stepovers with varying stress drop in models with a homogenous initial stress field. (a) Results for overlapping stepovers (overlapping configurations are shown in Figure 7). Symbols are explained in Figure 7. (b) Results for underlapping stepovers, with an offset angle of α =150°.